Synthesis of a CoO–ZnO nanocomposite and its study as a corrosion protection coating for stainless steel in saline solution

H.A. Almashhadani[1,2]

[1]*Dentistry Department, Al-Rasheed University College, Baghdad, 10011, Iraq*
[2]*College of technical engineering, The Islamic University, Najaf, 54001, Iraq*
**E-mail: Haideralmashhdani@alrasheedcol.edu.iq*

Abstract

A novel CoO–ZnO nanocomposite was synthesized by the photo irradiation method using a solution of cobalt and zinc complexes and used as a coating applied by electrophoretic deposition (EPD) for corrosion protection of stainless steel (SS) in saline solution. The samples were characterized using powder XRD, scanning electron microscopy (SEM) and electrochemical polarization. It was also found that the coating was still stable after conducting the corrosion test: it contained no cracks and CoO–ZnO nanocomposites clearly appeared on the surface. SEM showed that the significant surface cracking disappeared. XRD confirmed that CoO–ZnO nanocomposites comprised CoO and ZnO phases without any impurity. The SEM images of CoO–ZnO nanocomposites revealed the average particle size (23.66 nm). The corrosion behavior of the stainless steel in saline environment in the temperature range of 298–328 K was assessed by means of electrochemical techniques such as potentiodynamic polarization curves. The corrosion protection of the alloy increased with an increase in temperature from 99.97 to 99.99%, which indicates that the nanocomposite CoO–ZnO coating on the stainless steel surface is slightly affected by temperature. The results showed that CoO–ZnO nanocomposite provided powerful corrosion protection in saline solutions. The maximum protection efficiency was 99.99% in saline solutions at 328 K. The apparent activation energy (E_a) and pre-exponential factor (kinetic parameters) are calculated and discussed. Also, thermodynamic values such as the activation entropy (ΔS^*) and activation enthalpy (ΔH^*) were calculated.

Received: August 9, 2021. Published: September 17, 2021 doi: 10.17675/2305-6894-2021-10-3-26

Keywords: *nanocomposite, multi oxide, stainless steel, corrosion protection, electrophoretic deposition.*

1. Introduction

Stainless steel alloys are useful resources used in a variety of industrial and technological applications including food containers because of their good mechanical properties and corrosion resistance due to nickel and chromium they contain [1]. The corrosion resistance of stainless steels in various conditions depends on the creation of a lightweight adherent passive oxide layer. When the metal is exposed to aqueous media, such as acids and saline solutions, this surface layer dissolves completely due to electrochemical corrosion reaction

[2]. As a result, protecting stainless steel and its alloys from acidic and saline solutions is a significant challenge. Even so, many methods, such as coating, corrosion inhibitors, and anodizing processes, have been used to protect stainless steels in acid media from electrochemical corrosion reactions [3–5].

Among these methods, the coating process is widely used in industry to minimize the corrosion of steels that operate in contact with aggressive solutions [6]. Most common coatings are used to protect steel because of their adhesion, chemical resistance, mechanical and dielectric properties.

Oxide nanoparticles may have unique physical and chemical properties due to their high density and smaller size than bulky oxide particles. The semiconductor oxide properties arise due to the structural peculiarities of these compounds, specifically the point defects that give rise to the semiconducting nature [7].

Cobalt oxide (CoO) and zinc oxide (ZnO) are among the most widely used ceramic particle oxides as corrosion protection coatings [8, 9]. The employment of single oxide coatings has some limitations caused by the presence of cracks and pores in the coatings [10].

Composite or multi-oxide coatings have the capacity to combine the qualities of all of its constituent materials. To overcome the constraints of a single-oxide coating, the attributes of these coatings can be modified by altering the amounts of their components, such as the mix ratio of nanoparticles. Because of their low cost of production, ease of use, and high anticorrosive properties, metal oxide coatings are widely used for corrosion protection [11]. Metal oxide coatings provide excellent protection to alloys with outstanding corrosion, deformation, and corrosion resistance. Designing of bi- and tri-metal oxide composite coatings is an excellent option for increasing the service life of stainless steel [12].

For multifunctional applications, mixed metal oxide composites have shown notable chemical and physical capabilities compared to discrete metal oxide nanoparticles.

In this paper, CoO–ZnO nanocomposites were synthesized by the photo irradiation method and various methods were used: XRD to study their structure, SEM for surface morphology, and electrochemical tests for corrosion protection provided by the prepared ZnO–CoO nanocomposite coatings on stainless steel.

2. Experimental

2.1. Preparation of CoO–ZnO nanocomposites

All chemicals were used without any purification. At irradiation cell (Figure 1) was used to irradiate complexes of cobalt and zinc salt as sources of nanocomposites. An immersed UV light source with 125 W mercury medium pressure lamp was used with the maximum light intensity at a wavelength of 365 nm. The cell of photo-irradiation comprised a quartz tube like a jacket for the immersed UV light source in a solution of the nanocomposite. A Pyrex tube was employed as a reactor. To avoid a temperature rise caused by UV irradiation, the reactor was cooled with an ice bath.

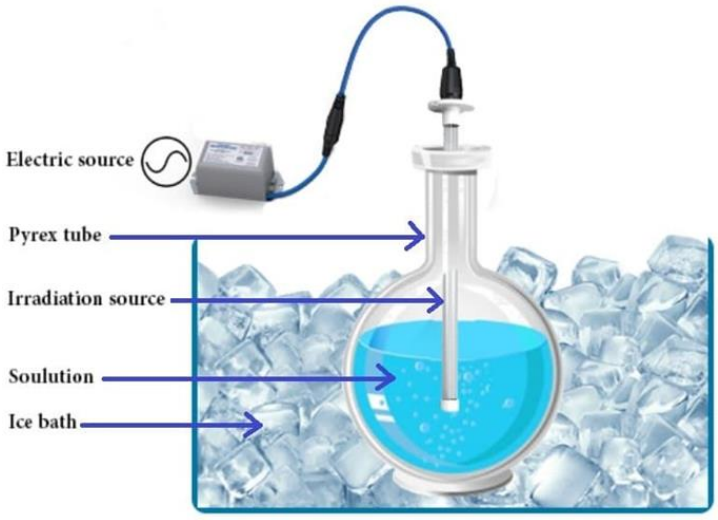

Figure 1. Diagram of photolysis cell.

Accordingly, 30 ml of 0.01 mole/L $Na_3Co(NO_2)_6$ and 30 ml of 0.01 mole/L $Zn(CH_3COO)_2$ were mixed together in a stoichiometric ratio (1:1). Then, 90 ml of 0.03 mole/L urea was added slowly (one drop per second) to the mixture and the latter was stirred for 15 min at room temperature. After that, the solution was irradiated by a photocell for 30 min. The nanocomposite precipitated as a red-brown (dark) powder; it was separated and washed several times with deionizing water (all the steps were done by centrifugation followed by decantation). The precipitate was dried in an oven at 100°C for 3 h and calcined at 400°C for 3 hours. Black-brown ZnO–CoO nanoparticles precipitated.

2.2. Electrophoresis deposition of emulsion solution (coating samples)

To apply the CoO–ZnO nanocomposite coating on stainless steel surfaces, a deposition cell device was used. The chemical composition of the stainless steel used was as follows: C 0.053, N 0.025, Cr 16.90, Ni 10.90, Mo 2.1, Si 0.75, Mn 1.24, Cu 0.20, P 0.03, S 0.027, B 0.002 (wt.%). The working electrode (Stainless steel) and large titanium sheet as a counter electrode were placed in an electrolyte (1 wt/v%) prepared by adding 1 g of the composite to 100 ml of distilled water. Electrophoretic deposition of the nanocomposite on the stainless steel was conducted at room temperature with stirring, under direct current power (DC) (15 V); the time was kept for 30 min. After deposition, the specimens were rinsed in distilled water and dried by a hair drier [13]

2.3. Characterization and electrochemical test

A number of techniques were used to characterize the CoO–ZnO nanocomposite sample. X-ray diffraction (XRD) Model D-5000 was used to investigate the composition of the specimens by using Cu-Kα radiation (λ=0.154 nm) source in θ/2θ. XRD measurements (10° to 80°) was performed at a measurement temperature (25°C) of ZnO–CoO nanocomposite [16]. A field emission scanning electron microscope (FE–SEM), model Jeol JSM-6010LV,

was used. A total of 20 μL was placed over a 300-mesh Cu grid and dried at room temperature.

Electrochemical experiments were performed using a WENKING M Lab. device (Germany). To study the corrosion of SS alloys, polarization curves were obtained. The polarization curves obtained involved cathodic and anodic areas. Extensive data might be collected from a careful investigation of each polarization region using an extrapolation technique to calculate both the corrosion current density (i_{corr}) and the corrosion potential (E_{corr}). A corrosion cell with a saturated calomel reference electrode (SCE), SS alloy as a working electrode, and a platinum rod auxiliary electrode was used [14]. Electrodes were placed into a 1 L corrosion cell with approximately 3.5% solution (35 g in 1 L of distilled water).

3. Result and Discussion

3.1. Potentiodynamic polarization studies

Figure 2a,b shows the potentiodynamic polarization curves obtained for SS alloys coated and uncoated by CoO–ZnO nanocomposite in saline media in a temperature range of 298–328 K. The kinetic parameters obtained from potentiodynamic polarization curves are listed in Table 1. It is clear that the i_{corr} values increase with temperature from 298 to 318 K, then decrease to 0.0348 μA/cm^2 at 328 K and decrease after the SS was coated by the CoO–ZnO nanocomposite. E_{corr} values for the coated SS alloy in saline media moved to a more active direction with an increase in temperature from 298 to 328 K, as shown in Table 1. Furthermore, E_{corr} in saline solution shifted towards the negative direction coating the SS by the CoO–ZnO nanocomposite, the maximum shift being 227 mV. This is more than 85 mV, which indicated that CoO–ZnO nanocomposite provides cathodic type protection [15, 16]. The Tafel slopes (b_a and b_c) are listed in Table 1. In saline solution, addition of the CoO–ZnO nanocomposite changes the b_a and b_c values, indicating a change in the mechanism of anodic and cathodic reaction, which indicated the mixed-type nature of the polarization process.

The percentage protection efficiency determined from Tafel polarization (%PE_T) is listed in Table 1. These values were calculated using the following equation [17]:

$$\%PE_T = \frac{i_{corr}^0 - i_{corr}}{i_{corr}^0} \times 100 \quad (1)$$

Where i_{corr}^0 and i_{corr} are the corrosion rates of SS uncoated and coated by the CoO–ZnO nanocomposite, respectively. The CoO–ZnO nanocomposite forms an excellent protective layer against corrosion in saline solution. The protection efficiency is not affected by temperature, indicating the stability of the coated layer on the metal surface. Based on the Stern–Geary equation, small polarization near the corrosion potential is performed to determine the corrosion resistance [18]:

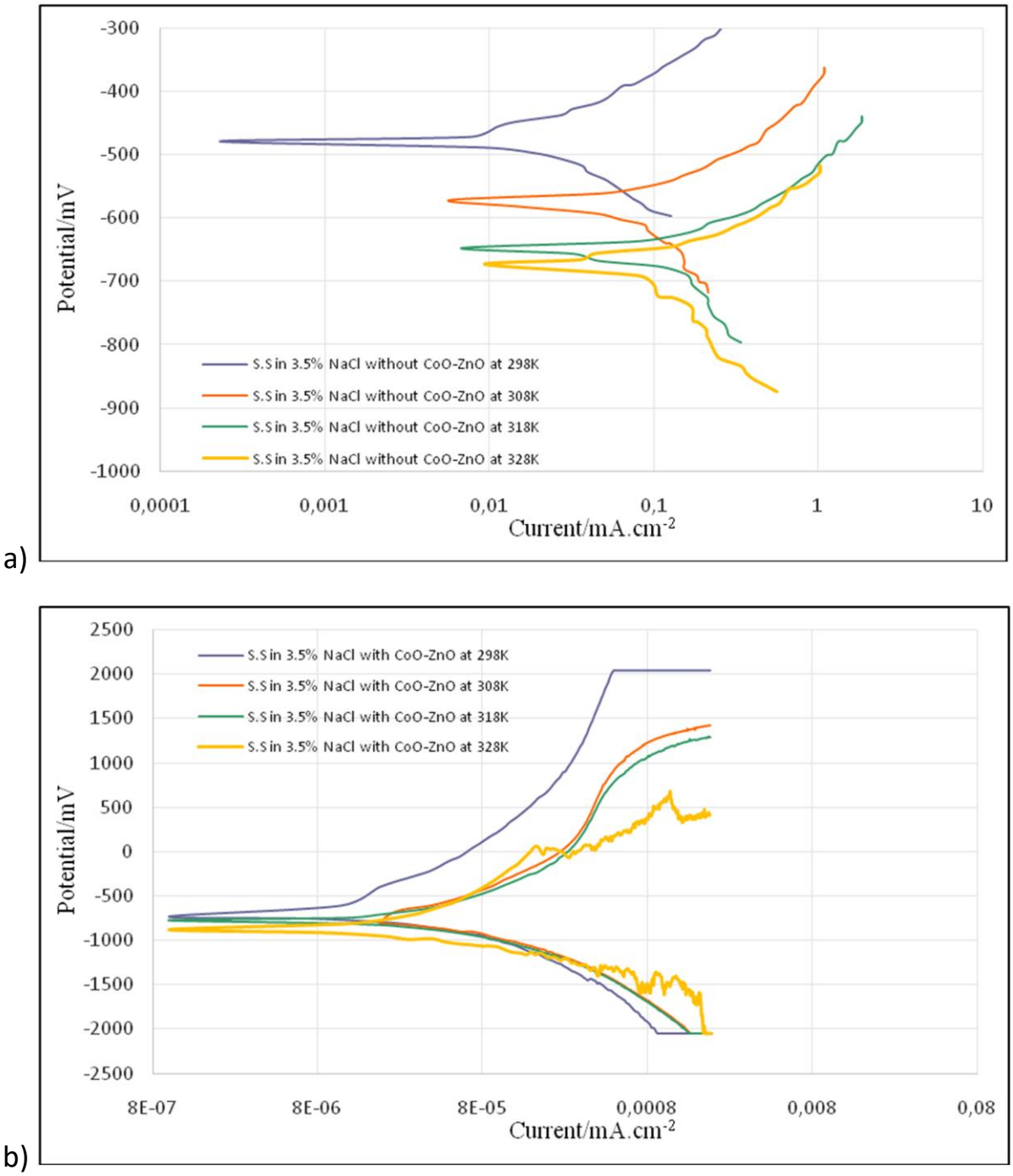

Figure 2. SS alloy polarization plots in saline medium in the 298–328 K range; a) without coating and b) after coating with the CoO–ZnO nanocomposite.

$$R_p = \frac{b_a b_c}{2.303(b_a + b_a)} \cdot \frac{1}{i_{corr}} \quad (2)$$

where R_p is the polarization resistance of the system. The percentage protection efficiency can be calculated from polarization resistance (%PE_R) by the following equation [19]:

$$\%PE_{\mathrm{R}} = \frac{R_{\mathrm{p}} - R_{\mathrm{p}}^{0}}{R_{\mathrm{p}}} \times 100 \quad (3)$$

Where R_{p}^{0} and R_{p} are the corrosion rates of SS without a coating and coated with the CoO–ZnO nanocomposite, respectively. The corrosion resistance decreases with temperature and increases after addition of the CoO–ZnO nanocomposite. The $\%PE_{\mathrm{P}}$ values are in good agreement with $\%PE_{\mathrm{T}}$.

Table 1. Corrosion kinetic parameters of SS alloys in saline at various temperatures.

Temp./K	**$-E_{\mathrm{corr}}$/mV**	**I_{corr}/μA·cm^{-2}**	**b_{a}/mV·dec^{-1}**	**$-b_{\mathrm{c}}$/mV·dec^{-1}**	**$\%PE_{\mathrm{T}}$**	**R_{p}/kΩ·cm^2**	**$\%PE_{\mathrm{R}}$**
Without coating							
298	478.5	20.64	159.6	161.5	–	1688.735	–
308	571.7	61.16	106.5	231.2	–	517.660	–
318	647.8	85.33	94.4	91.2	–	236.044	–
328	672.5	91.9	123.3	322.1	–	421.303	–
SS coated by the CoO–ZnO nanocomposite							
298	704.4	0.0197	1354.3	467.2	99.90	7.7×10^6	99.97
308	750.0	0.0406	985.5	570.6	99.93	3.9×10^6	99.98
318	766.0	0.0477	1019.8	631.6	99.94	3.6×10^6	99.99
328	874.2	0.0348	1314.0	405.4	99.96	3.9×10^6	99.99

3.2. Effect of temperature and kinetics studies

Commonly, temperature accelerates most chemical reactions. The effect of temperature on the corrosion reaction of SS alloy in saline solutions was studied in the range of 298–328 K. According to Table 1, the reaction rate (i_{corr}) increased with temperature. This behavior can be well understood using the Arrhenius equation (Eq. 4) and transition state equation (Eq. 5) [20]:

$$\log i_{\mathrm{corr}} = \frac{-E_{\mathrm{a}}}{2.303RT} + \log A \quad (4)$$

$$\log \frac{i_{\mathrm{corr}}}{T} = \log \frac{R}{Nh} + \frac{\Delta S^*}{2.303R} - \frac{\Delta H^*}{2.303RT} \quad (5)$$

Where E_{a} represents the apparent activation energy of the corrosion process, R is the gas constant (~8.314 J K^{-1} mol^{-1}), A is the pre-exponential factor, h is the Plank constant (6.626176×10^{-34} Js), N is the Avogadro's number (6.022×10^{23} mol^{-1}), ΔS^* is the entropy of activation, and ΔH^* is the enthalpy of activation. These equations can be plotted as log i_{corr} and log i_{corr}/T against reciprocal of absolute temperature, respectively (Figures 3 and 4). The

slopes and intercepts of these equations can be used to evaluate the kinetics parameters. The values of E_a and A were obtained from the slope ($-E_a/2.303R$) and intercept ($\log A$) of Eq. 4, respectively, while ΔH^* and ΔS^* were obtained from the slope of ($-\Delta H/2.303R$) and the intercept [$(\log(R/Nh)+(\Delta S/2.303R)$] of Eq. 5, respectively. The results are collected in Table 2.

Table 2. Kinetic parameters in the presence and absence of the coating.

Solution	ΔH^* (kJ·mol^{-1})	ΔS^* (kJ·mol^{-1}·K^{-1})	E_a (kJ·mol^{-1})	A Molec.cm^{-2}·s^{-1}
Without coating	37.03	–0.0934	39.626	1.41×1026
SS coated by the CoO–ZnO nanocomposite	13.12	–0.2315	15.71	8.62×1024

Values of ΔS^* which are presented in table (2) reflect the changes in the order and transition state orientation of the corrosion process of SS alloys, and the data in Table 2 shows the values of ΔS^* were affected by protected coating. Enthalpy of activation ΔH^* is a component of activation energy, for this note the values of ΔH^* are linked to the values of (E_a). The coated SS by CoO–ZnO nanocomposite has led to a decrease in the activation enthalpy ΔH^*. The apparent activation energy (E_a) decreased after coating SS by CoO–ZnO nanocomposite in comparison with uncoated SS alloy (Table 2).

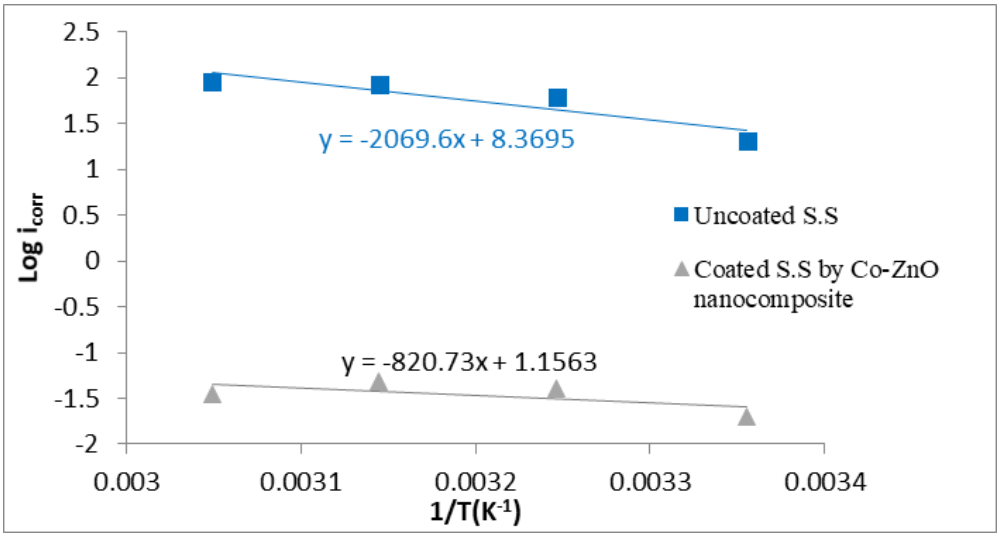

Figure 3. Arrhenius plot of $\log i_{corr}$ *versus* $1/T$ for the corrosion of SS in saline solution.

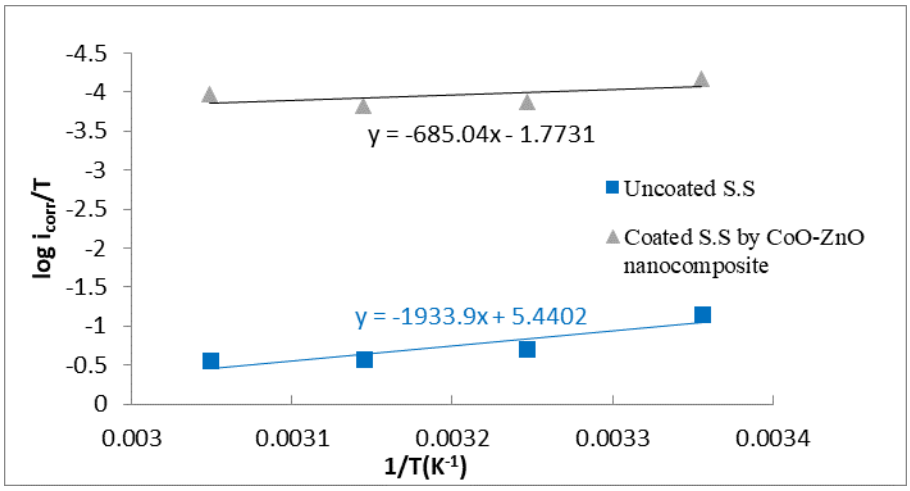

Figure 4. A plot of log i_{corr} *versus* 1/*T* for the corrosion of SS in saline solution.

This decrease is associated with the decrease in the number of corrosion sites on the surface of coated SS alloy approximately to 98%, according to the Arrhenius factor (*A*) which is usually used to refer to these sites.

3.3. Characterization and morphology of the prepared nanocomposite

Figure 5 shows the XRD patterns of prepared CoO nanoparticles, ZnO nanoparticles, and CoO–ZnO nanocomposites.

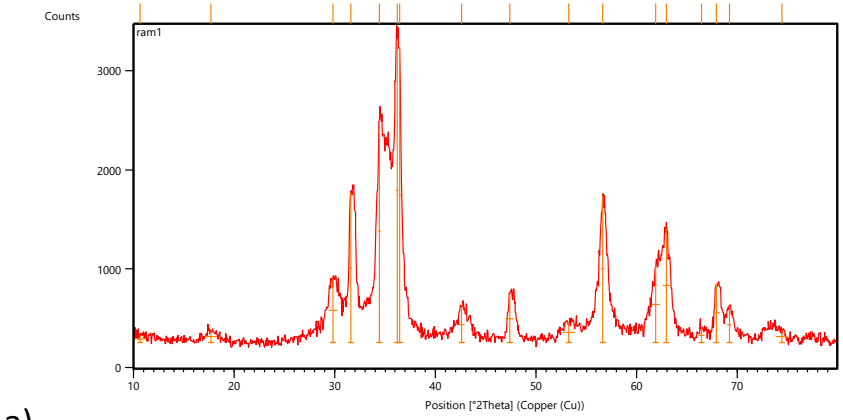

a)

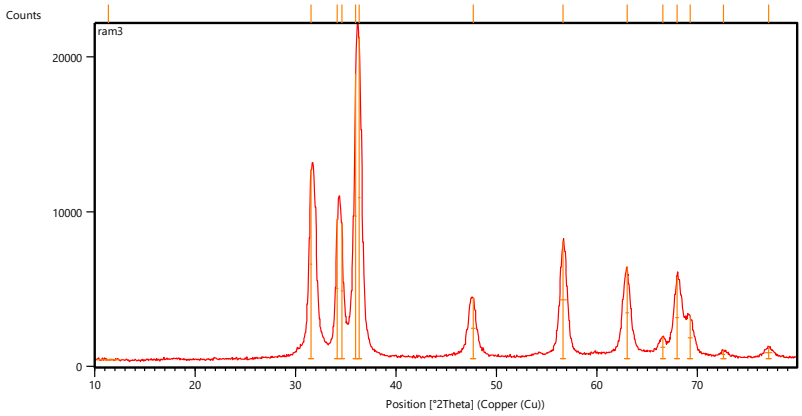

b)

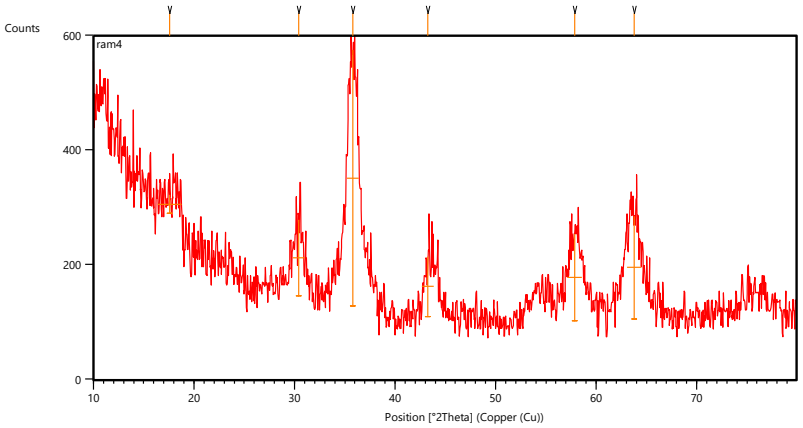

c)

Figure 5. XRD pattern of prepared a) CoO nanoparticles, b) ZnO nanoparticles, and c) CoO–ZnO nanocomposites.

There are significant amounts of line broadening that are characteristic of nanoparticles. The crystal size can be calculated according to the Debye–Scherrer formula [21].

$$D = \frac{k\lambda}{\beta \cos\theta} \tag{6}$$

Where $k = 0.9$ is the Scherrer constant, β is the full width at half maximum, λ is the wavelength of the Cu–Kα radiation, and θ is the angle obtained from 2θ values corresponding to the maximum intensity peak in the XRD pattern. Using the Scherrer equation, the grain size of the prepared cobalt oxide nanoparticles was calculated to be 43.3 nm. Zinc oxide nanoparticles were formed from pure ZnO nanoparticles with no impurity. The grain size of ZnO nanoparticles was measured to be 28.8 nm. The XRD pattern of CoO–ZnO nanocomposites confirms the formation of a sample with any impurity.

Scanning electron microscope (SEM) analysis was applied for studying the shape and size of the prepared CoO–ZnO nanocomposite. As shown in Figure 6, CoO with irregular shape was formed with an average particle size of 26.13 nm. Agglomerated particles were observed in Figure (6), which was to be expected since the applied synthesis method was performed by the surfactant-free route. For the ZnO was formed along with the other irregular morphology with an average particle size of 45.72 nm (Figure 7). Figure (8) shows the SEM images of the prepared CoO–ZnO nanocomposites. The applied synthesis method for the preparation of CoO–ZnO nanocomposites leads to the preservation of the morphology of CoO and ZnO nanoparticles. The SEM images of CoO–ZnO nanocomposites confirmed a slight decrease in the average particles size (23.66 nm) in the morphology in comparison with the shape and size of CoO and ZnO nanoparticles.

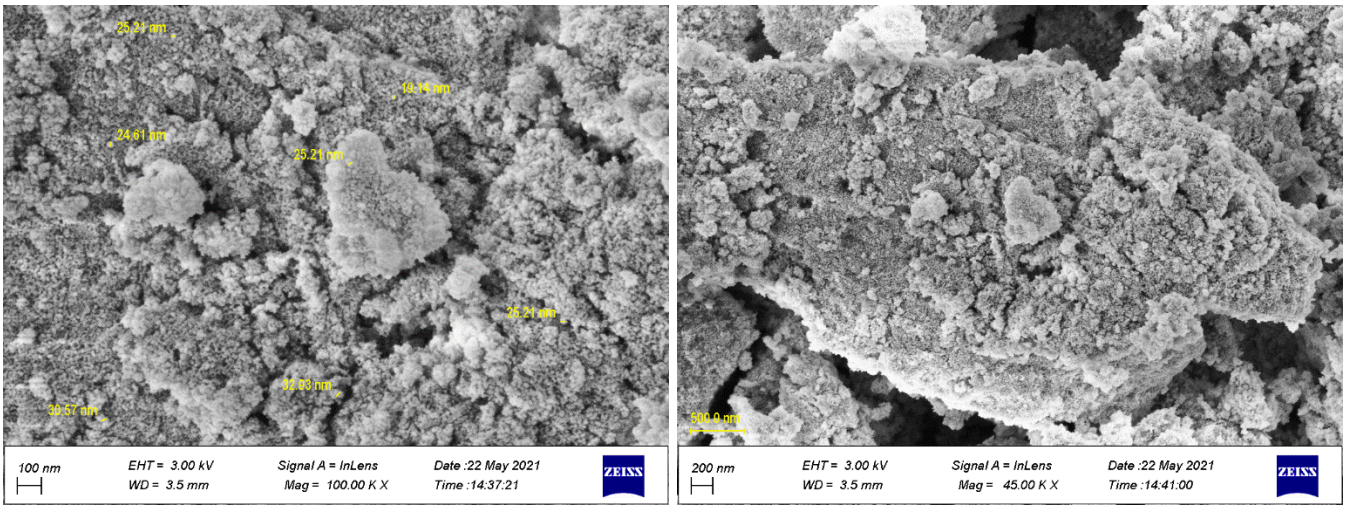

Figure 6. Scanning electron micrographs of CoO nanoparticles.

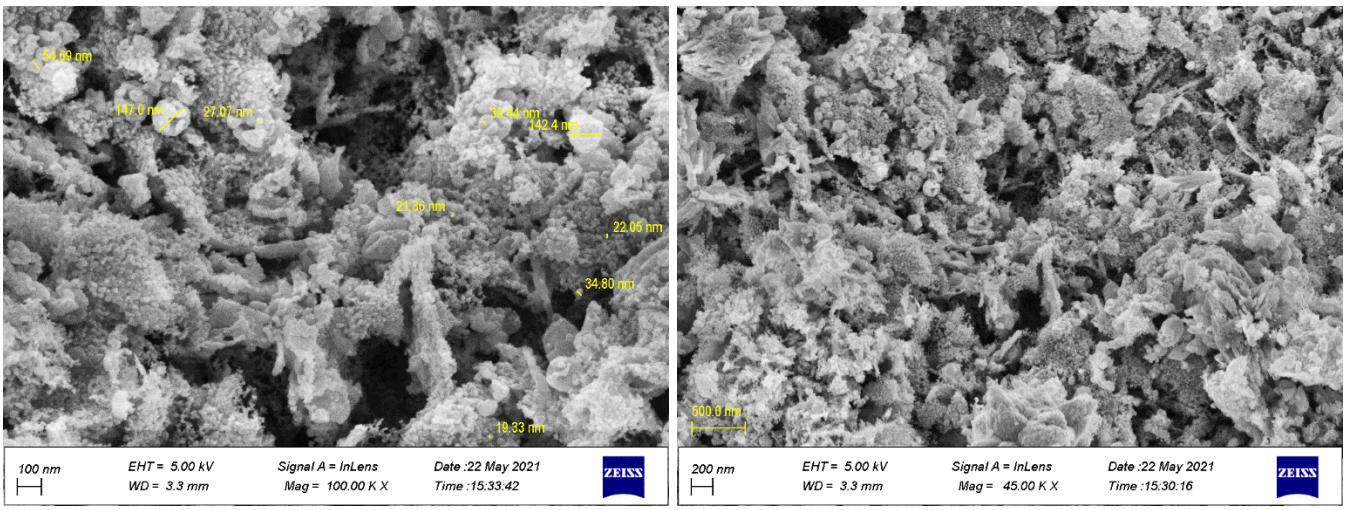

Figure 7. Scanning electron micrographs of ZnO nanoparticles.

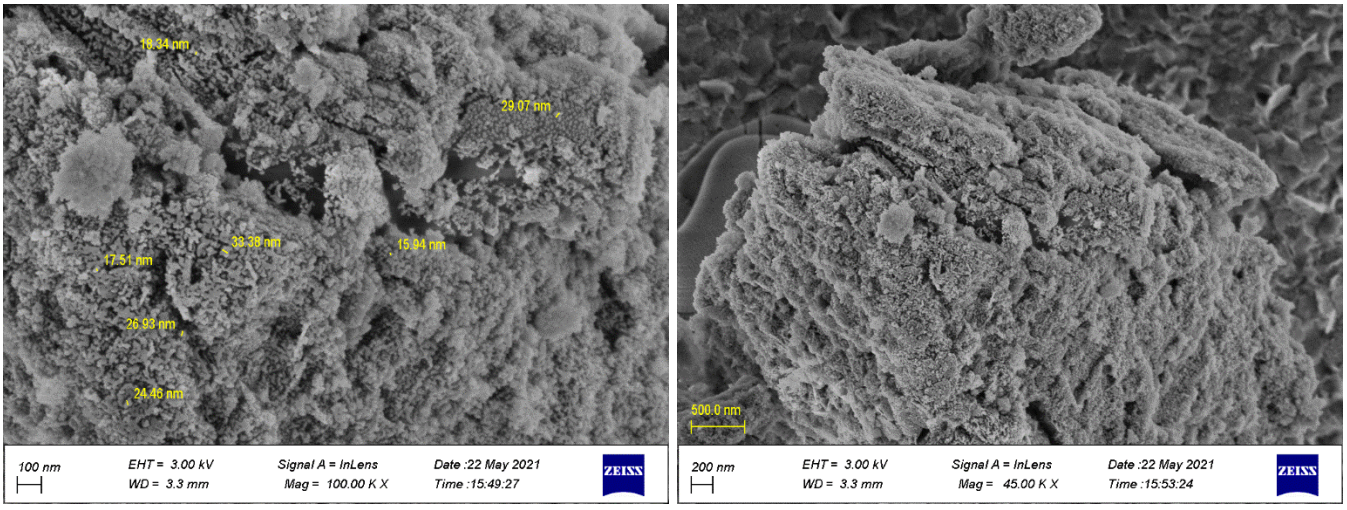

Figure 8. Scanning electron micrographs of the prepared CoO–ZnO nanocomposites.

3.4. Surface morphology of the nanocomposite coating

The SEM m icrographs of uncoated SS alloys and coated SS by CoO–ZnO nanocomposites are shown in Figure 9a,b. Figure 9a shows the uncoated morphology of the SS surface after conducting the corrosion test. The overall surface was covered in a brittle salt film with many fractures filled with corrosion products. The fractures formed were attributed to the inner stresses caused by the released gases mostly during cathodic reactions, or they could have formed as a result of the salt film.

The surface of coated SS after conducting the corrosion test in saline solution shows the coating is still stable after conducting the corrosion test without fractures and CoO–ZnO nanocomposites appear clearly on the surface.

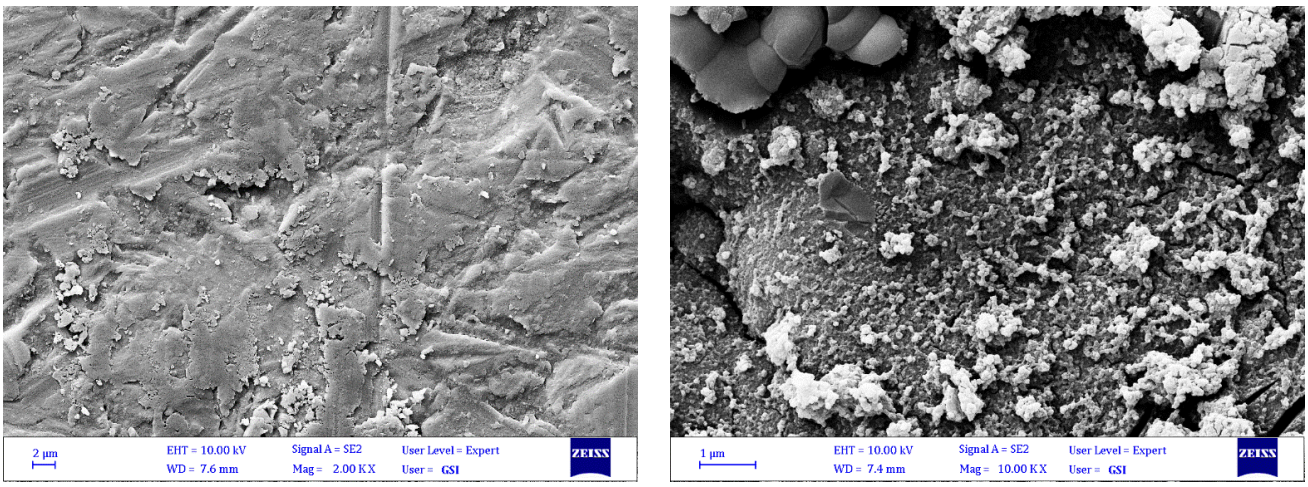

a) b)

Figure 9. Scanning electron micrographs of a) uncoated SS alloys and b) SS coated with CoO–ZnO nanocomposites.

Conclusion

It is found that using the photo irradiation method is a very reasonable, low cost, and effective approach for the successful preparation of the CoO–ZnO nanocomposite. The CoO–ZnO nanocomposite coating on SS alloy could significantly enhance the SS electrochemical properties compared with the uncoated SS. The CoO–ZnO nanocomposite coating acts as corrosion protection on SS alloys in saline solutions in the temperature range of 298–328 K. It was observed that the maximum protection efficiency was 99.99% in saline solutions at 328 K.

XRD revealed an arrangement of ZnO and CoO nanoparticles with an average crystallite size of 26 and 43.4 nm, respectively, and confirmed the formation of CoO and ZnO phases without any impurity.

The SEM images of CoO–ZnO nanocomposites confirmed a slight decrease in the average particle size (23.66 nm) in the morphology in comparison with the shape and size of CoO and ZnO nanoparticles.

References

1. A. Abdel-Gaber, B. Abd-El-Nabey, I. Sidahmed, A. El-Zayady and M. Saadawy, Kinetics and thermodynamics of aluminium dissolution in 1.0 M sulphuric acid containing chloride ions, *Mater. Chem. Phys*., 2006, **98**, 291–297. doi: 10.1016/j.matchemphys.2005.09.023
2. R. Nathiya, S. Perumal, V. Murugesan and V. Raj, Expired drugs: environmentally safe inhibitors for aluminium corrosion in 1 M H_2SO_4, *J. Bio Tribo Corros*., 2018, **4**, 1–13. doi: 10.1007/s40735-017-0120-1
3. G.K. Gomma and M.H. Wahdan, Schiff bases as corrosion inhibitors for aluminium in hydrochloric acid solution, *Mater. Chem. Phys*., 1995, **39**, 209–213. doi: 10.1016/0254-0584(94)01436-K
4. Y. Liu, D. Sun, H. You and J.S. Chung, Corrosion resistance properties of organic-inorganic hybrid coatings on 2024 aluminum alloy, *Appl. Surf. Sci*., 2005, **246**, 82–89. doi: 10.1016/j.apsusc.2004.10.040
5. L. Domingues, J. Fernandes, M.D.C. Belo, M. Ferreira and L. Guerra-Rosa, Anodising of Al 2024-T3 in a modified sulphuric acid/boric acid bath for aeronautical applications, *Corros. Sci*., 2003, **45**, 149–160. doi: 10.1016/S0010-938X(02)00082-3
6. H. Gerengi, K. Darowicki, G. Bereket and P. Slepski, Evaluation of corrosion inhibition of brass-118 in artificial seawater by benzotriazole using Dynamic EIS, *Corros. Sci*., 2009, **51**, 2573–2579. doi: 10.1016/j.corsci.2009.06.040
7. D.H. Hussain, H.I. Abdulah and A.M. Rheima, Synthesis and characterization of ɣ-Fe2O3 nanoparticles photo anode by novel method for dye sensitized solar cell, *Int. J. Sci. Res. Publ*., 2016, **6**, 26–31.
8. C.C. Ferreira, V.P. Ricci, L.L. de Sousa, N.A. Mariano and M.G.N. Campos, Improvement of titanium corrosion resistance by coating with poly-caprolactone and poly-caprolactone/titanium dioxide: potential application in heart valves, *Mater. Res*., 2018, **20**, 126–133. doi: 10.1590/1980-5373-MR-2017-0425
9. M.A. Almomani, M.T. Hayajneh and M.Y. Al-Daraghmeh, The corrosion behavior of AISI 304 stainless steel spin coated with ZrO2-gelatin nanocomposites, *Mater. Res. Express*, 2019, **6**, 0965c4. doi: 10.1088/2053-1591/aaeea0
10. M.R. Majdi, I. Danaee and S.S.S. Afghahi, Preparation and anti-corrosive properties of cerium oxide conversion coatings on steel X52, *Mater. Res*., 2017, **20**, 445–451. doi: 10.1590/1980-5373-MR-2016-0661
11. L. Shen, Y. Li, W. Zhao, K. Wang, X. Ci, Y. Wu, G. Liu, C. Liu and Z. Fang, Tuning F-doped degree of rGO: Restraining corrosion-promotion activity of EP/rGO nanocomposite coating, *J. Mater. Sci. Technol*., 2020, **44**, 121–132. doi: 10.1016/j.jmst.2019.09.043
12. S. Mandal, V. Das, M. Debata, A. Panigrahi, P. Sengupta, A. Rajendran, D. Pattanayak and S. Basu, Study of pore morphology, microstructure, and cell adhesion behaviour in porous Ti-6Al-4V scaffolds, *Emergent Mater*., 2019, **2**, 453–462. doi: 10.1007/s42247-019-00055-3

13. H. Almashhdani and K. Alsaadie, Corrosion Protection of Carbon Steel in seawater by alumina nanoparticles with poly (acrylic acid) as charging agent, *Moroccan J. Chem*., 2018, **6**, no. 3, 455–465. doi: 10.48317/IMIST.PRSM/morjchem-v6i3.6214
14. H.A. Abbas, K.A.S. Alsaade and H.A.Y. AlMAshhdan, Study the effect of cyperus rotundus extracted as mouthwash on the corrosion of dental amalgam, In IOP Conference Series, *Mater. Sci. Eng*., 2019, **571**, p. 012074. doi: 10.1088/1757-899X/571/1/012074
15. H.A. AlMashhadani and K.A. Saleh, Electro-polymerization of poly Eugenol on Ti and Ti alloy dental implant treatment by micro arc oxidation using as Anti-corrosion and Anti-microbial, *Res. J. Pharm. Technol*., 2020, **13**, 4687–4696. doi: 10.5958/0974-360X.2020.00825.2
16. H.A. AlMashhadani, Corrosion protection of pure titanium implant in artificial saliva by electro-polymerization of poly eugenol, *Egyptian J. Chem*., 2020, **63**, 2–3. doi: 10.21608/ejchem.2019.13617.1842
17. H.A. AlMashhadani and K.A. Saleh, Electrochemical Deposition of Hydroxyapatite Co-Substituted by Sr/Mg Coating on Ti-6Al-4V ELI Dental Alloy Post-MAO as Anti-Corrosion, *Iraqi J. Sci*., 2020, 2751–2761. doi: 10.24996/ijs.2020.61.11.1
18. A.S. Yaro, A.A. Khadom and H.F. Ibraheem, Peach juice as an anti-corrosion inhibitor of mild steel, *Anti-Corros. Meth. Mater*., 2011. doi: 10.1108/00035591111130497
19. B. Ramaganthan, M. Gopiraman, L.O. Olasunkanmi, M.M. Kabanda, S. Yesudass, I. Bahadur, A.S. Adekunle, I.B. Obot and E.E. Ebenso, Synthesized photo-cross-linking chalcones as novel corrosion inhibitors for mild steel in acidic medium: experimental, quantum chemical and Monte Carlo simulation studies, *RSC Adv*., 2015, **5**, 76675–76688. doi: 10.1039/C5RA12097G
20. H.A. Al-Mashhadani, M.K. Alshujery, F.A. Khazaal, A.M. Salman, M.M. Kadhim, Z.M. Abbas, S.K. Farag and H.F. Hussien, Anti-Corrosive Substance as Green Inhibitor for Carbon Steel in Saline and Acidic Media, in *J. Phys.: Conf. Ser*., 2021, **1818**, p. 012128. doi: 10.1088/1742-6596/1818/1/012128
21. U. Holzwarth and N. Gibson, The Scherrer equation versus the "Debye-Scherrer equation", *Nat. Nanotechnol*., 2011, **6**, 534–534. doi: 10.1038/nnano.2011.145

♦ ♦ ♦